

## $^{13}\text{C}$ NMR study of the metal-insulator and structural phase transition in the organic conductor (fluoranthenyl) $_2\text{PF}_6$

K. F. Thier and M. Mehring

2. Physikalisches Institut, Universität Stuttgart, Pfaffenwaldring 57, D-70550 Stuttgart, Federal Republic of Germany

(Received 8 October 1993; revised manuscript received 11 April 1994)

$^{13}\text{C}$  NMR measurements on single crystals of (fluoranthenyl) $_2\text{PF}_6$  at variable temperatures and for different orientations of the crystals with respect to the external field reveal strongly temperature-dependent Knight-shift anisotropies. Hyperfine-interaction tensors for the different carbon sites of the fluoranthene molecule were determined and are compared with molecular-orbital-type calculations. The temperature dependence of the paramagnetic spin susceptibility was determined through the metal-insulator transition. The spectra exhibit clearly a structural, as well as a metal-insulator, phase transition at and below 200 K. A detailed analysis of the temperature-dependent shift data leads to the determination of the temperature-dependent order parameter for both transitions.

### I. INTRODUCTION

NMR measurements on organic conductors have revealed important information about structural as well as electronic phase transitions in these highly anisotropic materials.<sup>1-4</sup> The local property of NMR spectroscopy allows us to determine site-selective hyperfine interactions on the atomic level, from which static as well as dynamic information about conduction electrons and phase transitions can be derived. The observed Knight shift is connected with the static susceptibility of the conduction electrons, and is therefore a direct measure of the density of states once the hyperfine interaction is known. From spin-lattice-relaxation data valuable information about fluctuations of the conduction electrons and how these scale with the susceptibility has been obtained.<sup>5-7</sup> A number of investigations have focused on tetracyanoquinodimethane (TCNQ) salts in the past. Here we present highly resolved  $^{13}\text{C}$  NMR data for one of the most highly one-dimensional radical ion organic conductors. For a review of the application of high-resolution NMR to organic conductors, see Ref. 8.

Radical salts of the fluoranthene molecule belong to a class of organic conductors with highly anisotropic conductivities in the metallic phase. The radical salts consist of stacks of positively charged molecules where the molecular plane is oriented perpendicularly to the stacking axis.<sup>9,10</sup> Between the stacks different types of anions (i.e.,  $\text{PF}_6^-$ ,  $\text{AsF}_6^-$ , and  $\text{ClO}_4^-$ ) stabilize the structure without introducing significant changes of structural and physical properties.<sup>11</sup> The highly anisotropic crystal structure leads to quasi-one-dimensional behavior of many electronic properties such as charge<sup>12</sup> and spin mobility.<sup>13</sup> From spin-diffusion measurements in single crystals,<sup>13</sup> it was concluded that (fluoranthenyl) $_2\text{PF}_6$  [abbreviated in the following by (FA) $_2\text{PF}_6$ ] is very likely the most one-dimensional radical cation salt known to date. All radical salts of this type exhibit a metal-insulator transition near 200 K. Because of the highly one-dimensional character of this material the metal-insulator transition is supposedly that of Peierls instability.

High-resolution  $^{13}\text{C}$  as well as  $^1\text{H}$  NMR techniques were applied before, and have demonstrated that site-selective proton and  $^{13}\text{C}$  Knight-shift tensors on the molecular level can indeed be observed.<sup>14-18</sup> Figure 1 shows the structure of the fluoranthene molecule and the assignment of the different carbon sites of the molecule. Due to a molecular mirror plane the primed and unprimed positions become magnetically equivalent. In the organic conductor, however, this symmetry can be broken by the crystal structure.

Above the metal-insulator transition the marked and unmarked sites of the molecule are observed still to be related by mirror symmetry, as is evident, e.g., from the corresponding  $^{13}\text{C}$  NMR spectra. Also, the dimerization seen in the crystal structure at room temperature does not lead to a splitting of the spectra. The reason for this is an inversion symmetry with respect to the anion positions. In the low-temperature phase these symmetries are broken, and all carbon sites in the unit cell have different magnetic surroundings. In this paper we extend earlier

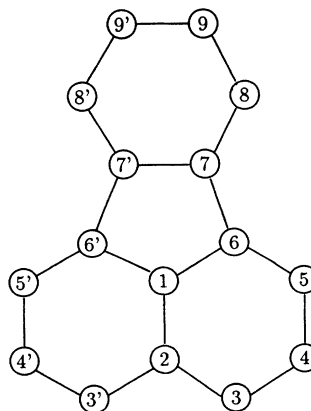


FIG. 1. Schematic structure of the fluoranthene molecule and assignment of the carbon positions.

measurements of the <sup>13</sup>C Knight-shift tensor<sup>15</sup> through the metal-insulator transition down to the insulating state. We will demonstrate in the following sections that important information can be derived from these data about the order parameter of the metal-insulator transition.

## II. EXPERIMENT

All measurements were carried out on single crystals of (FA)<sub>2</sub>PF<sub>6</sub> which were grown electrochemically from a solution of neutral fluoranthene and (TBA)PF<sub>6</sub>. The black needlelike crystals had sizes up to 0.5 × 1 × 10 mm<sup>3</sup>.

The spectra were recorded on a home-built triple-resonance spectrometer operating at a <sup>13</sup>C Larmor frequency of 46 MHz. Triple-resonance experiments were necessary to decouple <sup>13</sup>C-<sup>1</sup>H and <sup>13</sup>C-<sup>19</sup>F interactions. Polarization transfer from the protons was used not only to enhance the sensitivity but also to separate spectroscopically protonated from nonprotonated carbons. Cooling was performed with an Oxford CF1200 flow cryostat, and liquid nitrogen as a coolant.

## III. KNIGHT SHIFT, HYPERFINE COUPLING, AND SPIN DENSITY

The investigation of Knight shifts leads to important information about the electron distribution in organic conductors. In particular, <sup>13</sup>C NMR has proven to reveal important information about the conduction electron-spin density at different carbon sites of the corresponding molecules.<sup>14,15,17,19</sup>

### A. Knight shifts

The magnetic field at a particular nuclear site is in general different from the applied external field due to different magnetic interactions with the surrounding electrons. This leads to a shift in the NMR resonance frequency, described by the total second-rank shift tensor  $\vec{\delta}$  as represented by the following Hamiltonian:

$$\mathcal{H} = \mathcal{H}_0 + \gamma_n \hbar \vec{I} \vec{\delta} \mathbf{B}_0. \quad (1)$$

In systems with delocalized electron spins, it is convenient to separate the resonance shift  $\vec{\delta}$  into two contributions: the Knight shift  $\vec{K}$  and the chemical shift  $\vec{\sigma}$ :

$$\vec{\delta} = \vec{\sigma} + \vec{K}. \quad (2)$$

While  $\vec{\sigma}$  is due to close electronic shells (orbital shift), the term Knight shift  $\vec{K}$  is reserved here for the hyperfine interaction ( $\vec{A}$ ) with the conduction electrons. In first order, only the *zz* component of  $\vec{A}$  contributes to the shift:

$$\mathcal{H}_K = \sum_n \hbar \hat{I}_z A_{zz,n} \hat{S}_{z,n}. \quad (3)$$

In Eq. (3) the summation must be performed over all electrons in the conduction band. The hyperfine coupling tensor  $\vec{A}$  can be separated into an isotropic part which reflects all *s*-orbital contributions, whereas the dipolar part is due to contributions of *p*-type and higher angular momentum orbitals:

$$\vec{A} = a_{\text{iso}} \vec{E} + \vec{A}', \quad (4)$$

where  $\vec{E}$  is the unit tensor.

In an externally applied field the effective spin polarization is due to the paramagnetic susceptibility of the delocalized electrons. Combining the hyperfine interaction with the paramagnetic susceptibility leads to the anisotropic Knight shift

$$K_{zz} = \frac{\Delta\omega}{\omega} = (\hbar\gamma_n\gamma_e)^{-1} \chi_s A_{zz}. \quad (5)$$

When applying Eq. (5), we will assume that the susceptibility  $\chi_s$  is isotropic, whereas  $A_{zz}$  contains the full orientational dependence of the Knight shift. If the absolute value of  $\chi_s$  is known, one can determine the complete symmetric part of the hyperfine tensor for all carbon sites in the molecule by applying Eq. (5) for different magnetic-field orientations.

$\vec{K}$  is usually isotropic for normal metals because of either cubic symmetry or the *s* character of the conduction electrons. Organic conductors show quite a different behavior: the conductivity usually arises from delocalized  $\pi$  orbitals which have nodes at the sites of the carbon positions leading to a larger dipolar contribution to  $\vec{K}$ . However, the isotropic part of  $\vec{K}$  also does not vanish. On the contrary, it is rather significant because of core-polarization effects.<sup>14</sup>

### B. Experimental results

Because of the quasi-one-dimensional structure of the crystal and the planar structure of the molecules, we expect one of the principal axes of all shift tensors to be oriented parallel to the stacking axis, which again is parallel to the *a* axis of the crystal. The other two tensor axes then will lie in the molecular plane.

With this model in mind, it is reasonable to rotate the crystal around its *a* axis with the rotation axis oriented perpendicular to the external field  $B_0$ . So-called rotation plots of  $\vec{\delta}$  result which can be fitted to a  $\cos 2\phi$  dependence. From this type of analysis of  $\vec{\delta}$ , the principal axes of the two tensor components in the molecular plane can be determined. An additional spectrum taken with the external field along the stacking axis allows the determination of the third tensor component.

In Fig. 2 the temperature dependence of the <sup>13</sup>C spectrum for two different orientations of the external field is shown. All shift values are reported here with respect to TMS (tetramethylsilane). The left part shows the spectra with the external field parallel to the stacking axis. The Knight shift drops rapidly at the phase transition, and the total spectrum collapses to a narrow range of a few ppm. We take the shift values of 90 K as a reference for the chemical shift, since all paramagnetic contributions are reduced to a very small fraction at this temperature. The Knight shift is then determined as the difference between the high-temperature and low-temperature shifts.

In Fig. 3 it is shown that all Knight shifts scale very precisely with each other over the whole temperature range. This leads to two important conclusions.

(i) Hyperfine and chemical shift interaction along the stacking axis do not change with temperature, and the

temperature dependence of the line shifts is entirely due to a variation in the paramagnetic susceptibility.

(ii) All carbon sites contribute to the same conduction band. A single conduction-band picture is therefore appropriate.

From (i) we conclude that the temperature dependence of the Knight shift yields directly the temperature dependence of the paramagnetic susceptibility, and the hyperfine couplings can be determined from the different slopes of the straight lines in Fig. 3. The constant

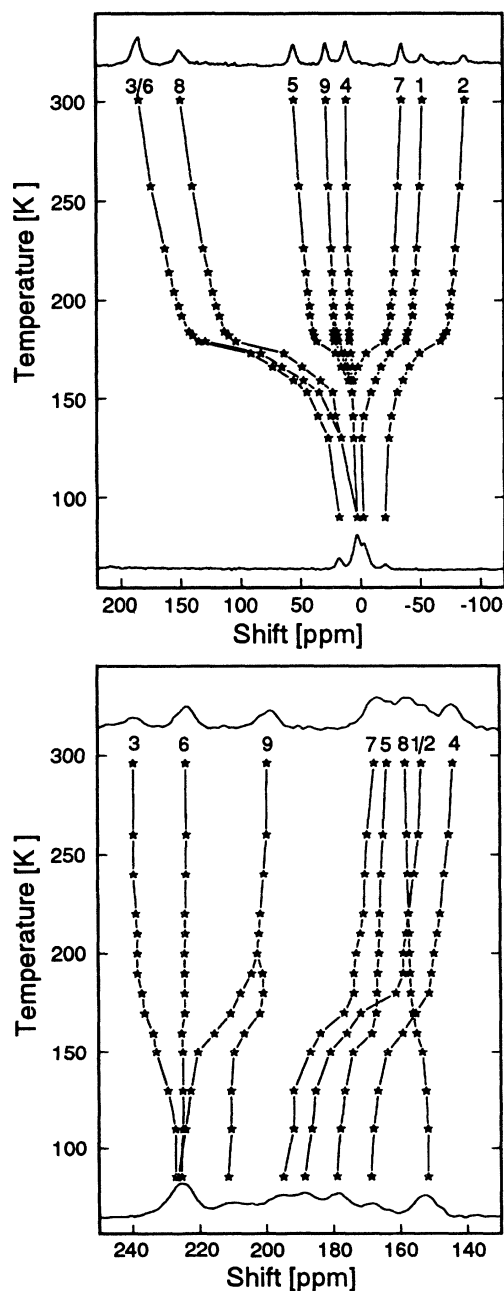


FIG. 2. Temperature dependence of the different  $^{13}\text{C}$  lines with the orientation of the  $a$  axis (top) and the  $c^*$  axis (bottom) parallel to the external field.

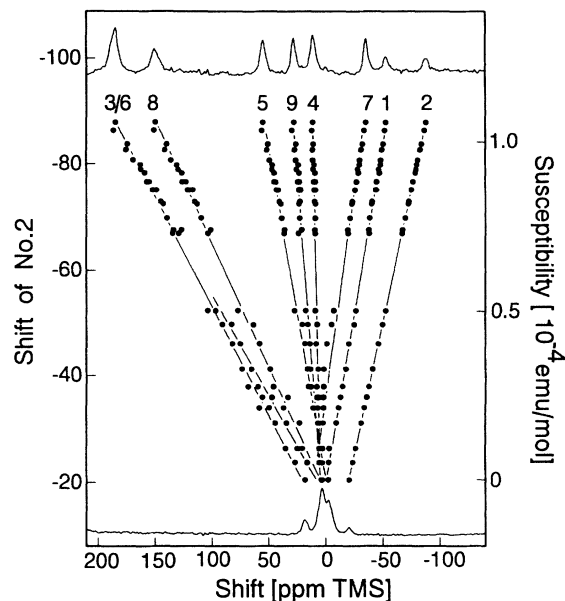


FIG. 3. Scaling of the line shift at position 2 with the line shifts at all other positions. The linear scaling over the full temperature range indicates constant hyperfine couplings above and below the phase transition, and allows us to separate hyperfine interaction and susceptibility.

hyperfine interaction over the whole temperature range supports the view that hyperfine interaction is first of all a molecular property, and is not affected very much by the delocalization of the electrons.

With the external field oriented perpendicular to the stacking axis, the Knight shifts are much smaller. This is due to a much smaller hyperfine coupling.

Figure 4 shows examples of rotation plots at room temperature and at 90 K. Spectra were taken every  $8^\circ$ – $12^\circ$ . At room temperature we obtain the same results as before.<sup>15</sup> There, however, the determination of the Knight-shift values was only possible by making several assumptions about the Knight shift and the chemical shift. Here we use the 90-K shifts as reference values for the chemical shift in order to extract the Knight shift from the total shift.

We note that it is rather difficult to resolve all the lines at low temperatures, because the spectral dispersion is much smaller. Another difficulty concerns the increase in the number of peaks below the phase transition due to a reduction in crystal symmetry. At room temperature a maximum number of 16 different carbon sites are expected due to the crystal symmetry, resulting in eight magnetically inequivalent spectral peaks. Below the phase transition, however, a maximum of 64 different carbon sites would be expected due to crystal symmetry. Spectral broadening severely limits the resolution at low temperature, which allows us to resolve only up to 17 spectral peaks. Two equivalent sets are expected if interactions between different stacks and with the anions can be neglected, which implies that the corresponding positions on the FA dimer are still equivalent at low temperature.

Moreover, there is a rotation of the stacks according to the low-temperature crystal structure which leads to a rotation of the shift tensors around the  $a$  axis. Because this rotation is only about  $\pm 4.5^\circ$ , the two inequivalent peaks resulting from this cannot be resolved and we are able to observe only a broadening of the lines. Except for position 9, where we can indeed resolve this splitting, we have approximated the unresolved double peaks by using a larger linewidth. To enhance the resolution and assure the assignment of the positions, we have taken additional low-temperature rotation plots with very short cross-polarization times ( $t_{\text{CP}} < 100 \mu\text{s}$ ), thus reducing the number of lines in the spectrum to only the number of protonated positions in the molecule.

The average shift tensor resulting from this fitting procedure had the same principal axis orientation as the room-temperature shift tensor. This confirms the hypothesis that the shift tensors in the low-temperature phase are simply rotated by the same angle as the molecular stacks. The peak corresponding to positions 9 and 9' splits into two different peaks as mentioned before. This is due to inequivalent chemical shifts indicating the broken symmetry below the structural phase transition. This splitting will be discussed in more detail in the Sec. III C.

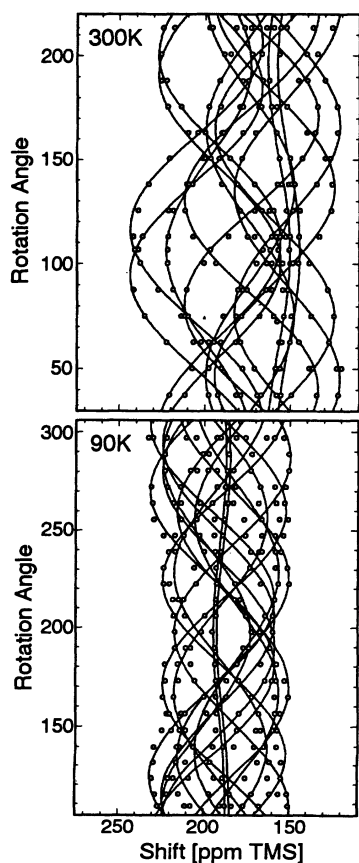


FIG. 4. Angular dependence of the line shifts for a rotation of the external field in the molecular plane. Top:  $T=300$  K; bottom:  $T=90$  K. Rotation angles are given in degree.

TABLE I. Orientation of the hyperfine interaction tensors at the different molecular positions. The 33 component is always parallel to the stacking axis, whereas the 11 and 22 components lie in the molecular plane. The last column lists the angle between  $A_{11}$  and the  $c^*$  direction.

Pos.	$A_{33}$ (MHz)	$A_{22}$ (MHz)	$A_{11}$ (MHz)	$\phi(A_{11}, c^*)$
1	-5.8	-3.4	-3.0	$\pm 90^\circ$
2	-7.5	-3.9	-3.4	$\pm 90^\circ$
3	20.8	0.5	0.9	$\pm 11^\circ$
4	1.1	-2.8	-3.0	$\pm 59^\circ$
5	6.9	-1.2	-1.4	$\pm 59^\circ$
6	19.0	0	-0.2	$0^\circ$
7	-5.7	-3.6	-2.2	$\pm 29^\circ$
8	16.9	0.7	1.1	$\pm 85^\circ$
9	2.9	-2.4	-1.1	$\pm 25^\circ$

In order to determine the hyperfine interaction, we used low-temperature data as a reference for the chemical shift, as discussed above. This was not possible, however, for position 9, and we had to estimate the chemical shift from the temperature-dependent data above the phase transition for this position. For the determination of absolute values of the hyperfine tensor from the Knight-shift data, one needs to know the paramagnetic susceptibility. Since all Knight shifts scale with each other, as demonstrated in Fig. 3, we are able to derive all site-selective hyperfine tensors by using  $\chi_s = 1.06 \times 10^{-4}$  emu/mol as an absolute value for the paramagnetic susceptibility which has been measured very accurately by Köbler, Gmeiner and Dormann.<sup>20</sup> The hyperfine tensors obtained by such an analysis are listed in Table I. We can distinguish between three different kinds of tensors. The hyperfine tensors of positions 3, 6 and 8 exhibit large anisotropy and consist mainly of a single component parallel to the stacking axis. It is also for these carbon positions that x-ray structure predicts the largest overlap of  $\pi$  orbitals between neighbor molecules. For carbons 1, 2, and 7 we find more isotropic tensors with all principal axis values negative. The protonated positions 4, 5, and 9 finally all have positive components along the stacking

TABLE II. Separation of  $A$  into the isotropic coupling  $a_{\text{iso}}$  and dipolar part  $A'$ . The last column indicates the deviation from axial symmetry with regard to the stacking axis.

Pos.	$a_{\text{iso}}$ (MHz)	$A'_{33}$ (MHz)	$A'_{22}$ (MHz)	$A'_{11}$ (MHz)	$\frac{ A_{11} - A_{22} }{A_{33}}$
1	-4.1	-1.7	0.7	1.1	0.069
2	-4.9	-2.6	1.0	1.5	0.067
3	7.4	13.4	-6.9	-6.5	0.019
4	-1.6	2.7	-1.2	-1.4	0.182
5	1.4	5.5	-2.6	-2.8	0.029
6	6.3	12.7	-6.3	-6.5	0.011
7	-3.8	-1.9	0.2	1.6	0.246
8	6.2	10.7	-5.5	-5.1	0.023
9	-0.2	3.1	-2.2	-0.9	0.448

axis, and negative couplings in the molecular plane.

It is interesting to note that all hyperfine tensors are approximately axially symmetric. This supports *a posteriori* this assumption made earlier in the analysis of the hyperfine tensor.<sup>15</sup> Axial symmetry is of course expected from the conjecture made earlier that the  $p_z$  orbitals play the dominant role in the formation of the conduction band. Small deviations from this axial symmetry are caused by the protons bound to the aromatic rings. In Table II the hyperfine tensors are separated into their isotropic and anisotropic parts. The value in the last column reflects the deviation from axial symmetry. Besides a few exceptions (positions 7 and 9) it turns out to be rather small indeed. The knowledge of the exact hyperfine tensors will be important for the calculation of the spin-density distribution at the carbon sites of the molecule and for the interpretation of the relaxation data.

### C. Spin density: Comparison of theory and experiment

In this section we address the question of how to obtain information about the wave-function of the conduction electron band. In view of a linear combination of atomic orbitals (LCAO) picture it is expected that the  $p_z$  orbitals of the carbon atoms form the basis for the conduction band. Since the  $^{13}\text{C}$  hyperfine interaction is directly (although in a complicated manner) related to the spin density in the  $p_z$  orbital, valuable information about this spin density, i.e., the LCAO coefficient, can in principle be obtained. However, this requires that reliable information about the spin density can be extracted from the hyperfine interaction. Unfortunately this is by no means a trivial task. There exist some empirical models relating hyperfine interaction and spin density. McConnell found, e.g., a linear dependence between the isotropic part of the proton hyperfine interaction and the spin density on the neighboring carbon site.<sup>21</sup> Karplus and Fraenkel derived a similar relation between the spin densities in the  $p_z$  orbital and the isotropic carbon hyperfine interactions.<sup>22</sup> Both models were already applied to the fluoranthene radical salts,<sup>16,15</sup> but conflicting results were obtained. In particular, the Karplus-Fraenkel relation can lead to completely unreasonable spin-density values when applied without care. The problem derives from the fact that the isotropic hyperfine interaction reflects only very indirectly the spin density in the  $p_z$  orbitals because it is dominated by core polarization of the  $s$  electrons. The observation that the dipolar part of the hyperfine tensor reflects more directly the spin densities in the  $p_z$  orbitals was therefore very useful, and allowed us to estimate the spin density from a simple point dipole model.<sup>15</sup>

Rather than applying a simple empirical rule for the spin density, here we present a more appropriate approach in that we compare the experimental hyperfine tensors with molecular-orbital (MO) calculations directly. For this reason we have applied a Hartree-Fock-type semiempirical MO calculation of the INDO (intermediate neglect of differential orbitals) type to a fluoranthene radical cation. We used the molecular structure given in Ref. 10. Corrections due to the 2:1 stoichiometry in the

radical salt were made by dividing the spin-density and hyperfine couplings by a factor of 2.

The advantage of this procedure lies in the fact that the complete wave function and therefore the hyperfine interaction is obtained directly. Moreover, if reliable agreement between calculated and measured hyperfine interactions is achieved, the values for  $\rho$  obtained from the calculations could in turn be compared with  $\rho$  values derived empirically from the experimental hyperfine data. The results are presented in a pictorial way in Fig. 5, where the filled circles belong to positive and the open circles to negative hyperfine couplings or spin densities, respectively. One obtains good qualitative topological agreement when isotropic and anisotropic couplings are compared separately. Unfortunately, a deviation of the absolute values between theoretical and experimental hyperfine values is observed. This is certainly a deficiency of the MO program because different scaling factors are necessary for the isotropic and dipolar parts of  $A$ . Whereas the theoretical isotropic hyperfine coupling is 50% larger than the experimental values, the calculated dipolar contribution is smaller than experimentally observed, and must be scaled by a factor of about 1.67 in order to achieve agreement with the experimental results. Nevertheless it is revealing that the order of magnitude and moreover the topological distribution of the hyperfine interaction on the molecule comes out in close agreement between MO theory and experiment. Moreover, this proves the molecular character of the conduction electron band.

A possible explanation for the deviation between MO

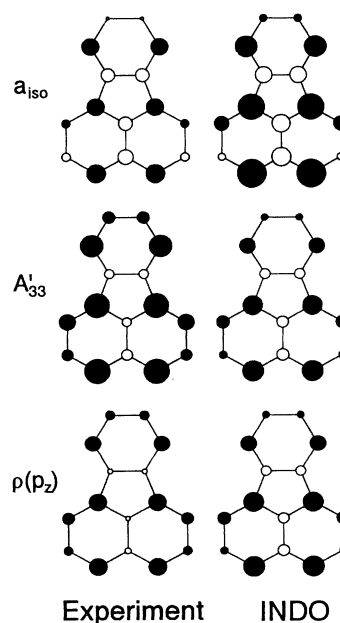


FIG. 5. Comparison of  $a_{\text{iso}}$ ,  $A_{33}^1$ , and the spin density in the  $p_z$  orbital obtained from experiment (left) and INDO calculations (right). The area of the circles is proportional to the magnitude of the corresponding value.

theory and the experimental data could also be due to the intermolecular interaction, i.e., a solid-state effect. It would therefore be desirable to perform band-structure calculations of, e.g., the local density type in order to clarify this point.

#### IV. THE PHASE TRANSITION: STRUCTURAL AND METAL-INSULATOR TRANSITION

Fluoranthene radical salts are often referred to as model systems for a Peierls instability, named after R. E. Peierls who described the instability of one-dimensional systems against formation of a charge-density wave (CDW).<sup>23</sup> Together with the CDW state a gap opens in the electronic states.<sup>24</sup> The opening of a gap below 180 K has been observed in conductivity<sup>12</sup> and susceptibility<sup>20</sup> measurements. Characteristic nonlinear effects of a CDW could also be seen in more recent conductivity measurements.<sup>25</sup> The gross features of the <sup>13</sup>C spectra around the transition temperature also show the opening of a gap which is seen in the rapid continuous decrease of the Knight shift toward zero. The details around the transition are, however, more complicated since, 20 K above the electronic phase transition, a structural phase transition takes place. The structural transition affects the unit-cell parameters only very weakly. But a slight rotation of the fluoranthenyl molecules around their stacking axis is introduced accompanied by a reorientation of the anions.<sup>26</sup>

Knight- and chemical-shift measurements provide us with tools which allow us to detect both phase transitions separately. The Knight shift, being sensitive to the paramagnetic susceptibility, gives information about the electronic degrees of freedom, whereas the chemical shift is sensitive to structural changes. In Sec. III we showed how to separate these two contributions.

In order to be more specific, let us take a look at Fig. 2, where a splitting of the spectral peaks assigned to position 9 is seen below 200 K. We note that the very slow relaxation of these lines compared to their neighbor lines makes it possible to trace these lines easily, despite the large overlap.

This splitting cannot be explained by a change in hyperfine coupling, but rather a rotation of the shift tensor must be invoked. This is therefore a fingerprint of the structural phase transition, where the splitting is caused by the onset of the stacking rotation, which is known from the x-ray crystal structure.<sup>26</sup> It leads to a loss of symmetry, and positions 9 and 9' in the molecule become distinguishable. By plotting the shift difference of the spectral peaks versus temperature, an order-parameter curve for the structural phase transition can be derived. It will be shown in the following that this can be distinguished from the evolution of the electronic gap. This conjecture is supported by the fact that changes occur only at a position which is closest to atomic positions of neighboring molecules, and only those principal axes of  $\vec{\delta}$  which lie in the molecular plane are affected.

The susceptibility obtained from the Knight-shift data can be interpreted in a similar way to the bulk susceptibility in Ref. 20, where the decrease of the static suscepti-

bility with decreasing temperature is assigned to a reduction in the density of states according to a theory of Lee, Rice, and Anderson.<sup>27</sup> A more applicable treatment was introduced by Johnston,<sup>28</sup> who described the fluctuation effects by a pseudogap  $\Delta$  which already exists above the real metal-insulator transition temperature. Following Johnston<sup>28</sup> and Köbler, Gmeiner, and Dormann,<sup>20</sup> we fitted the temperature-dependent Knight shift to

$$\frac{K(T)}{K_0} = \int_A^\infty \frac{x}{(x^2 - A^2)^{1/2}} \frac{e^x}{(e^x + 1)^2} dx, \quad (6)$$

with  $x = E/k_B T$  and  $A = \delta_{\text{eff}}/k_B T$ , where  $\delta_{\text{eff}}$  is the effective gap generated by fluctuations, as discussed in Ref. 27.  $K_0$  was extrapolated from the metallic regime and corresponds to  $\chi_\infty = 1.2710^{-4}$  emu/mol.

In Fig. 6 both the effective gap and the difference between the chemical shift values of positions 9 and 9' are plotted versus temperature. The temperature dependence shows two different values for  $T_c$ . For a detailed understanding of these two different phase transitions, it would be desirable to derive the critical exponent from the order-parameter curve. However, this is not trivial because the procedure is very sensitive to a change in  $T_c$  which is not known exactly. Nevertheless we have attempted it. The lines drawn in Fig. 6 correspond to

$$\Delta_{\text{eff}}(T) = \Delta_0 (1 - t_p)^{\beta_p}, \quad (7)$$

with  $t_p = T/T_p$  and

$$\Delta\sigma(T) = \Delta\sigma_0 (1 - t_s)^{\beta_s}, \quad (8)$$

with  $t_s = T/T_s$ , where we distinguish between the Peierls (index  $p$ ) and the structural (index  $s$ ) transition temperatures. The following values are obtained:  $\beta_p = 0.257$ ,  $\Delta(0)/k_B = 835$  K and  $\beta_s = 0.496$ ,  $\Delta\sigma_0 = 20.3$  ppm, with

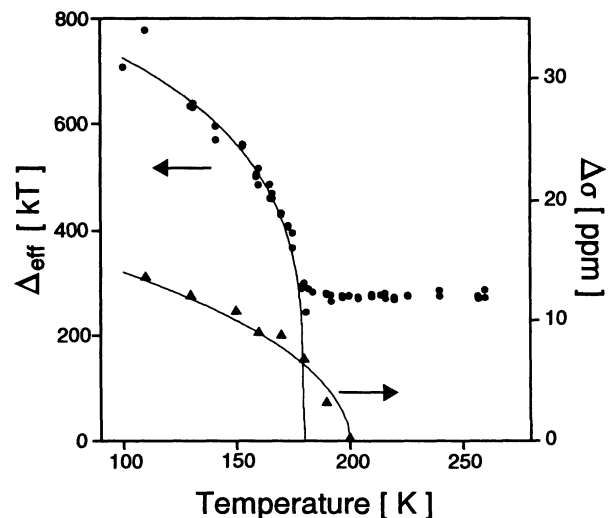


FIG. 6. Temperature dependence of the effective electronic gap (circles) derived from the Knight-shift analysis and chemical-shift splitting (triangles), corresponding to the metal-insulator and structural phase transitions.

$T_p = 180$  K and  $T_s = 200$  K, respectively.

We believe that the proximity of the structural and the metal-insulator transition is not accidental. It is well known that three-dimensional Coulombic coupling is necessary to drive a quasi-one-dimensional system into a Peierls state at finite temperatures.<sup>3</sup> The electronic phase transition therefore occurs only when the structural transition introduces enough three-dimensional coupling. Similar behavior has been observed in other low-dimensional systems such as TTF-TCNQ (where TTF is an acronym for tetrathiofulvalene).<sup>3</sup> Finally, we point out that Ilacovac *et al.*<sup>29</sup> also recently observed these separate transitions in diffuse x-ray scattering. In addition, we have investigated the temperature dependence of the relaxation time  $T_1$  for different <sup>13</sup>C sites. The orientational dependence of the relaxation rate can be accounted for fully by the hyperfine tensors reported here. Its temperature dependence, however, reflects the dynamic features of the phase transition and is not related in a simple or modified Korringa-type relation to the Knight-shift data. We will therefore present these results in a separate publication.

#### V. SUMMARY

We have demonstrated that a complete temperature dependent analysis of <sup>13</sup>C Knight-shift spectra in the quasi-one-dimensional organic conductor (fluoranthenyl)<sub>2</sub>PF<sub>6</sub> through the metal-insulator transition allows us to separate chemical (orbital) shift tensors from Knight-shift tensors, and to determine both contri-

butions to the line shift separately. Moreover, the Knight-shift could again be separated into temperature-dependent paramagnetic susceptibility and the temperature-independent hyperfine tensor for each nuclear carbon site on the fluoranthene molecule. The hyperfine tensors are nearly axially symmetric, and their anisotropy explains partially the large Korringa enhancement factors.<sup>30,31</sup>

A MO calculation of the hyperfine interaction tensor for the fluoranthene radical cation is in reasonable agreement with the experimental data, leading to the conclusion that a single conduction-band picture applies which basically consists of a linear combination of the singly occupied molecular orbital. This is further supported by the correlated scaling of all Knight-shift values for different temperatures.

The detailed analysis of the chemical and Knight-shift data has allowed us to observe the structural transition at 200 K separately from the metal-insulator transition at 180 K. Details of the electronic gap opening were derived from the temperature dependence of the Knight-shift data led to the temperature dependence of the order parameter. No line broadenings due to CDW formation could be resolved.

#### ACKNOWLEDGMENTS

We are grateful to J. Klein for preparing the samples, and to M. Helmle for many interesting discussions. The project was supported in part by the Fonds der Chemischen Industrie.

- <sup>1</sup>E. Ehrenfreund, E. F. Rybaczewski, A. F. Garito, and A. J. Heeger, *Phys. Rev. Lett.* **28**, 873 (1972).
- <sup>2</sup>G. Soda, D. Jerome, M. Weger, J. Alizon, J. Gallice, H. Robert, J. M. Fabre, and L. Giral, *J. Phys. (France)* **38**, 931 (1977).
- <sup>3</sup>D. Jerome and H. J. Schulz, *Adv. Phys.* **31**, 299 (1982).
- <sup>4</sup>T. Takahashi, D. Jerome, F. Masin, J. M. Fabre, and L. Giral, *J. Phys. C* **17**, 3777 (1984).
- <sup>5</sup>C. Bourbonnais, R. T. Henriques, P. Wzietek, D. Königeter, J. Voiron, and D. Jerome, *Phys. Rev. B* **44**, 641 (1991).
- <sup>6</sup>C. Bourbonnais, *J. Phys. I (France)* **3**, 143 (1993).
- <sup>7</sup>P. Wzietek, F. Creuzet, C. Bourbonnais, D. Jerome, K. Bechgaard, and P. Batail, *J. Phys. I (France)* **3**, 171 (1993).
- <sup>8</sup>M. Helmle and M. Mehring, in *Nuclear Spectroscopy on Charge Density Wave Systems*, edited by Tilman Butz (Kluwer Academic, Amsterdam, 1992).
- <sup>9</sup>Ch. Kröhnke, V. Enkelmann, and G. Wegner, *Angew. Chem.* **92**, 941 (1980).
- <sup>10</sup>V. Enkelmann, B. S. Morra, Ch. Kröhnke, and G. Wegner, *Chem. Phys.* **66**, 303 (1982).
- <sup>11</sup>V. Enkelmann and K. Göckelmann, *Ber. Bunsenges, Phys. Chem.* **91**, 950 (1987).
- <sup>12</sup>Th. Schimmel, W. Riess, G. Denninger, and M. Schwoerer, *Ber. Bunsenges, Phys. Chem.* **91**, 901 (1987).
- <sup>13</sup>G. G. Maresch, doctoral thesis, Universität Stuttgart, 1987.
- <sup>14</sup>M. Mehring and J. Spengler, *Phys. Rev. Lett.* **53**, 2441 (1984).
- <sup>15</sup>D. Königeter and M. Mehring, *Phys. Rev. B* **39**, 6361 (1989).
- <sup>16</sup>F. Hentsch, M. Helmle, D. Königeter, and M. Mehring, *Phys. Rev. B* **37**, 7205 (1988).
- <sup>17</sup>G. Zimmer, A. C. Kolbert, M. Mehring, F. Rachdi, P. Bernier, and M. Almeida, *Phys. Rev. B* **47**, 763 (1993).
- <sup>18</sup>A. C. Kolbert, G. Zimmer, F. Rachdi, P. Bernier, M. Almeida, and M. Mehring, *Phys. Rev. B* **46**, 574 (1992).
- <sup>19</sup>F. Rachdi, T. Nunes, M. Ribet, P. Bernier, M. Helmle, M. Mehring, and M. Almeida, *Phys. Rev.* **45**, 8134 (1992).
- <sup>20</sup>U. Köbler, J. Gmeiner, and E. Dormann, *J. Magn. Magn. Mater.* **69**, 189 (1987).
- <sup>21</sup>H. M. McConnell and D. B. Chesnut, *J. Chem. Phys.* **28**, 107 (1958).
- <sup>22</sup>M. Karplus and G. K. Fraenkel, *J. Chem. Phys.* **35**, 1312 (1961).
- <sup>23</sup>R. E. Peierls, *Quantum Theorie of Solids* (Oxford University Press, London, 1956), Sec. 135.
- <sup>24</sup>For a review on this topic and further references, see P. Monceau, *Synth. Met.* **41-43**, 3103 (1991).
- <sup>25</sup>W. Riess, W. Schmid, J. Gmeiner, and M. Schwoerer, *Synth. Met.* **42**, 2261 (1991).
- <sup>26</sup>V. Enkelmann, *Synth. Met.* **42**, 2547 (1991).
- <sup>27</sup>P. A. Lee, T. M. Rice, and P. W. Anderson, *Phys. Rev. Lett.* **31**, 462 (1973).

<sup>28</sup>D. C. Johnston, *Phys. Rev. Lett.* **52**, 2049 (1984).

<sup>29</sup>V. Ilakovac, S. Ravy, J. P. Pouget, W. Riess, W. Brütting, and M. Schwoerer, *J. Phys. (Paris) IV* **3**, 137 (1993).

<sup>30</sup>M. Mehring, in *Low Dimensional Conductors and Supercon-*

*ductors*, Vol. 155 of *NATO Advanced Study Institute, Series B: Physics*, edited by D. Jerome and L. G. Caron (Plenum, New York, 1987).

<sup>31</sup>M. Helmle and M. Mehring (unpublished).